Proceedings of the
Annual Stability Conference
Structural Stability Research Council
Denver, Colorado, March 22-25 2022

Cold-formed steel corrugated sheet shear wall with special energy dissipation bracing

Yu Cheng[1], Tian Yu[2], Zhang Wenying[3]

Abstract
Recent research showed that cold-formed steel shear walls with corrugated steel sheathing demonstrated high strength, high initial lateral stiffness but low ductility and thus were not suitable for applied in the high seismic risk zone. The paper presents a solution by installing a special energy dissipation bracing (EDB) to improve the ductility of the corrugated sheet sheathed shear walls. The EDB can be tuned according to the CFS shear wall base performance to achieve the highest post-peak deflection capacity, therefore the seismic ductility will be significantly improved. To prove the concept and analyze the feasibility of the new EDB, a test program of a total of 9 full-scale shear walls was conducted. The test results indicated that the corrugated steel sheathed shear walls using the EDB with optimal parameters demonstrated an improved high ductility without a significant reduction in shear strength and initial lateral stiffness. Details of the test program and general results are present in this paper.

Keywords
Cold-formed steel; Shear walls; Energy dissipation bracing.

1. Introduction

Cold-formed steel (CFS) structures have been used in low- and mid-rise residential and commercial buildings due to its advantage of high strength, quick construction, cost effectiveness, non-combustibility (Franklin et al. 2020), etc. The CFS framed shear walls as the primary lateral force resisting system in CFS buildings were investigated by several researchers (Serrette et al. 1996; Shamim et al. 2010; Vieira and Schafer 2013; Peterman and Schafer 2014; Ye et al. 2016; Selvaraj and Madhavan 2018). One of the main factors impacting the structural performance of CFS shear walls is the panel materials which commonly include oriental strand boards (OSB), plywood boards, gypsum boards and flat steel sheets. However, the combustibility of the wood-based panel sheathed shear walls and the low shear strength of flat sheet sheathed shear walls obstruct the use of the CFS shear walls with conventional panel materials in mid- and high-rise buildings. A potential solution is to use corrugated steel sheets as the panel material. It has been proven that CFS shear walls with corrugated steel sheets have significantly higher

[1] Professor, University of North Texas, <cheng.yu@unt.edu>
[2] Graduate Research Assistant, Beijing University of Technology, < bjutcety@163.com >
[3] Assistant Professor, Beijing University of Technology, <wenyingchangan@163.com>

lateral resistance and initial stiffness than those of walls sheathed by wood-based panels and flat steel sheets (Fülöp and Dubina 2004; Stojadinovic and Tipping 2007; Yu 2013). However, the test results also indicated that the shear walls with corrugated steel sheathing had poor ductility (Yu et al. 2016, 2018). In order to improve the ductility of CFS shear walls with corrugated steel sheathing, Yu et al. (2016, 2018) and Zhang et al. (2018) conducted a series of cyclic tests for CFS shear walls with different slits configuration. The results showed that with a proper slit pattern in the corrugated sheathing, the corrugated steel sheathed shear wall could yield significantly improved ductility while maintaining a high level of shear strength. However, the opening on the corrugated sheathing could reduce the fire rating of the wall and allow penetration of moisture. The method of creating openings in corrugated sheathing for improving ductility may not be accepted by the code officials.

This paper presents a new attempt to improve the ductility of the corrugated sheet sheathed CFS shear walls without negative impacts to the wall's fire and moisture resistances. A test program was recently conducted at the University of North Texas aimed at investigating the seismic performance of corrugated sheet sheathed CFS shear walls with a special energy dissipation bracing (EDB). The bracing consisted of threaded rods, rod ends, coupling nuts, plate holders with bolt holes and a dog bone shape steel plate with long-slotted bolt holes that could allow the plate to slide before bearing loads. Fig. 1 illustrates the details of the EDB. The concept is to let the brace provide additional stiffness and lateral resistance strength immediately after the shear wall maxed out its capacity and started to lose its shear strength. The task of the EDB is not to increase the nominal strength of the shear wall but rather to provide additional shear strength in the post-peak stage. It was expected that the EDB would prevent instant loss of shear wall strength after peak load and increase the ductility and the deformation capacity of the shear walls. Fig. 2 shows the photo of actual EDB. Slotted holes were used in the holding plates, so that the free displacement (sliding distance) could be controlled and modified to allow the EDB to be engaged in load bearing at a specified displacement. EDB also provides additional energy dissipation capacity to the shear wall. The energy dissipation mechanism of the EDB relies on the deformation and material yielding of the dog bone shape thin plate.

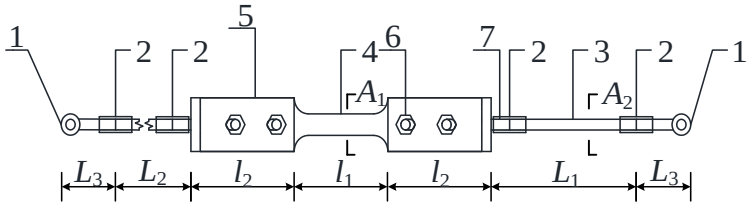

1-Rod end 2-Coupling nuts 3-Threaded rod 4-Dog bone shape plate 5-Holder 6-Bolts 7-Connector
Figure 1: The construction of energy dissipation bracing

Figure 2: The photograph of energy dissipation bracing

2. Test Program

2.1 Test Setup

The full-scale shear wall tests were conducted on 4.88 m (16 ft.) span, 3.66 m (12 ft.) steel reaction testing frame with one 156 kN (35 kip) capacity hydraulic actuator. The force was applied to the top track of the wall horizontally through a load beam. An 89 kN (20 kip) load cell was placed between the actuator shaft and the load beam to measure the applied force. The load beam was attached to the wall's top track via No. 14 hex washer head (HWH) self-drilling screws. The out-of-plane displacement of shear wall was restricted by the lateral supports placed on both sides of load beam. Five displacements (the horizontal displacement at the top of the wall, and the vertical and horizontal displacements of the bottom of the two chord studs) were measured by displacement transducers. Fig. 3 illustrates the shear wall test setup.

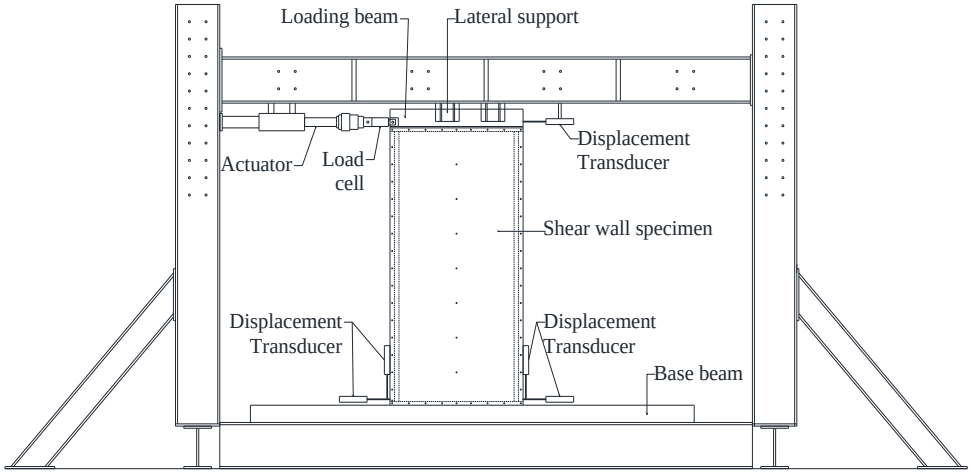

Figure 3: Front view of test setup

2.2 Test procedure

The lateral load was applied to the top of wall by using displacement-based protocols. The monotonic loading procedure followed ASTM E564 Standard Practice for Static Load Test for Shear Resistance of Framed Walls for Buildings (ASTM 2012a). The cyclic tests used the Consortium of Universities for Research in Earthquake Engineering (CUREE) protocol with a

0.2 Hz loading frequency in accordance with Method C in ASTM E2126 (ASTM 2012b). In order to investigate the seismic behavior of specimens at a relatively large deflection range, a new cyclic loading protocol was developed (referred as UNT protocol, shown in Fig.4) in this project and applied to one test. The new UNT protocol would enable investigation of up to +10.4% drift for a 2.44 m (8 ft.) tall wall.

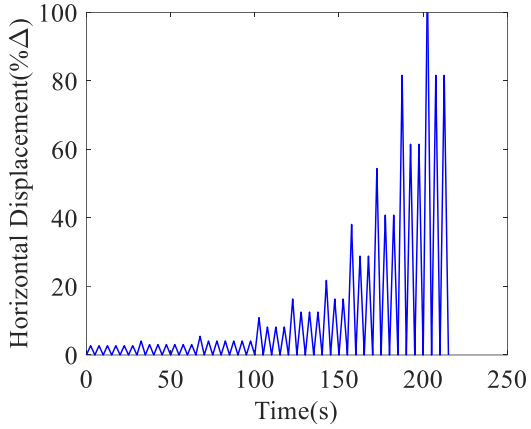

Figure 4: Diagram of the new UNT loading protocol

2.3 Test Specimens

The test program included two type of shear walls: CFS shear walls with EDB and without EDB. Those EDBs had 4 different sliding distances [0 mm, 12.5 mm (1/2 in.), 19.05 mm (3/4 in.), 25.4 mm (1 in.)] for parametric study. The test matrix is presented in Table 1. The test specimens are labeled as follows: SW represents Shear Wall; 4×8 represents the wall size (width × height) in feet; M represents monotonic loading and C indicates cyclic loading; the number after letter "M" or "C" represents the sliding distance in hundredths inches, e.g., 050 means 12.70 mm (0.50 in.); NB represents wall specimen without EBD; test specimen ends with "H" represents an adoption of the UNT loading protocol.

In this research, all shear walls were 2.44 m (8 ft.) high and 1.22 m (4 ft.) wide (2:1 aspect ratio). The CFS framing members were standard Steel Stud Manufactures Association (SSMA) structural studs (345 MPa 350S162-68) and tracks (345 MPa 350T125-68). The boundary studs were back-to -back studs fastened together with a pair of No.12×25.4 mm (1 in.) HWH self-drilling screws spaced at 152.4 mm (6 in.) on center. One single stud was installed at the middle of the shear wall frame. Four Simpson Strong Tie S/HD15S (Simpson Strong Tie, Pleasanton, California) hold-downs were installed to the boundary studs of cyclic test specimens and three same hold-downs were installed to the boundary studs of monotonic tests. As with traditional shear walls, two hold-downs were installed to the bottom of the shear walls without EDB to connect the shear walls to the foundation. The hold-downs were attached to the inside boundary stud by No.14×25.4 mm (1 in.) HWH self-drilling screws. For studs having punch-outs at the hold-down locations, additional welding around the edge of the punch-out was used to strengthen the hold-downs to stud attachment. Two 12.5 mm (1/2 in.) diameter bolt holes were drilled in the sidewall of hold-downs for anchoring the EDB. Two bolts with 12.5 mm (1/2 in.) diameter [ASTM325 (ASTM 2015)] were used to connect EDB to hold-downs. Fig. 5 shows that the detail of connection between hold-down and EDB.

Table 1: Tests matrix

Wall Label	Test Protocol	Sliding Distance of EDB (mm)
SW4×8-MNB	Monotonic	--
SW4×8-M100	Monotonic	25.40
SW4×8-M075	Monotonic	19.05
SW4×8-M050	Monotonic	12.70
SW4×8-CNB	CUREE Cyclic	--
SW4×8-C075	CUREE Cyclic	19.05
SW4×8-C050	CUREE Cyclic	12.70
SW4×8-C000	CUREE Cyclic	0
SW4×8-C050H	UNT Cyclic	12.70

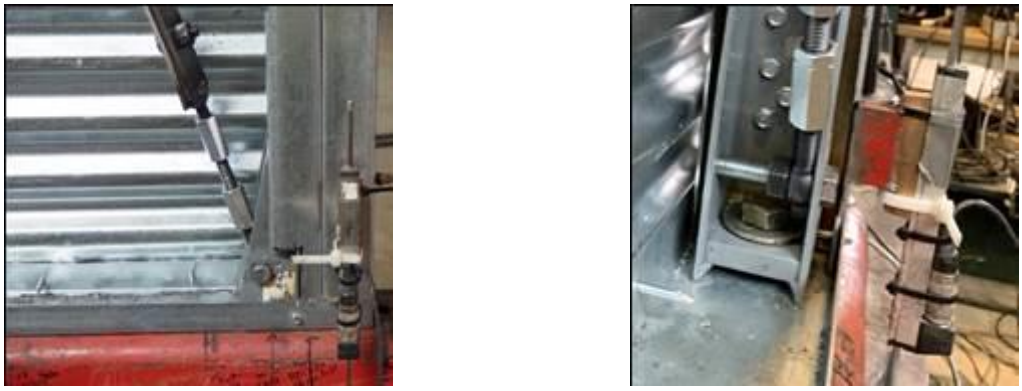

(a) (b)

Figure 5: The connection between hold-down and EDB (a) front view; (b) side view

All shear walls used the same sheathing material: Vulcraft 0.6C (Vulcraft, Florence, South Carolina), 14.3-mm rib height, 0.873-mm thick, 938-mm wide, 1220-mm long corrugated steel sheet with a nominal thickness of 0.873 mm as shown in Fig. 6. The sheathing was installed on one side of each specimen using No.12×25.4 mm (1 in.) HWH self-drilling screws. To accommodate the corrugation profile of sheathing, the spacing of screws was 127 mm (5 in.) along the horizontal seams of sheets, 127 mm (5 in.) along the wall perimeter, and 254 mm (10 in.) along interior stud. For all specimens, the corrugation of sheathing was placed in the horizontal direction. In each wall, the sheathing was composed of three corrugated steel sheets. Two 15.9 mm (5/8 in.) diameter ASTM A325 bolts [ASTM325 (ASTM 2015)] were used to anchor the bottom track to the base beam. Two 15.9 mm (5/8 in.) diameter ASTM A325 bolts [ASTM325 (ASTM 2015)] were used for fixing the hold-downs to the base beam. Fig.7 shows the detail of four dog bone shape steel plate configurations. Fig.8 shows the layout and details of test specimens.

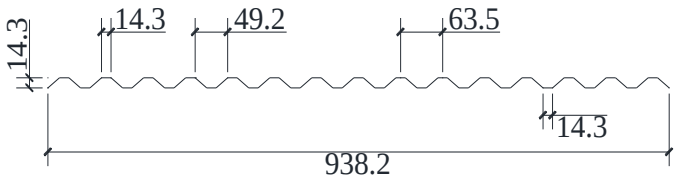

Figure 6: Dimension of corrugated steel sheets (unit: mm)

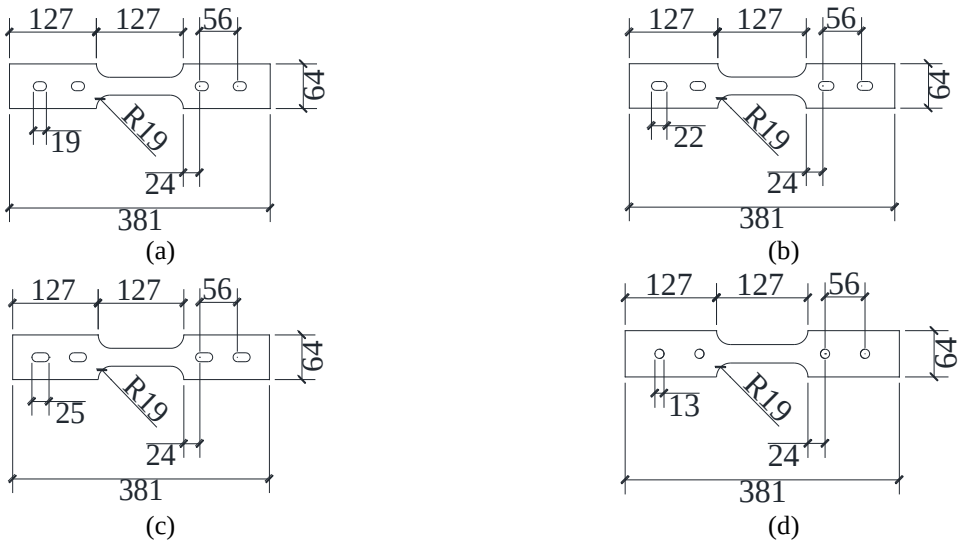

Figure 7: Dog bone shape steel plate configurations (a) 12.5mm; (b) 19.05mm; (c) 25.4mm; (d) 0mm;

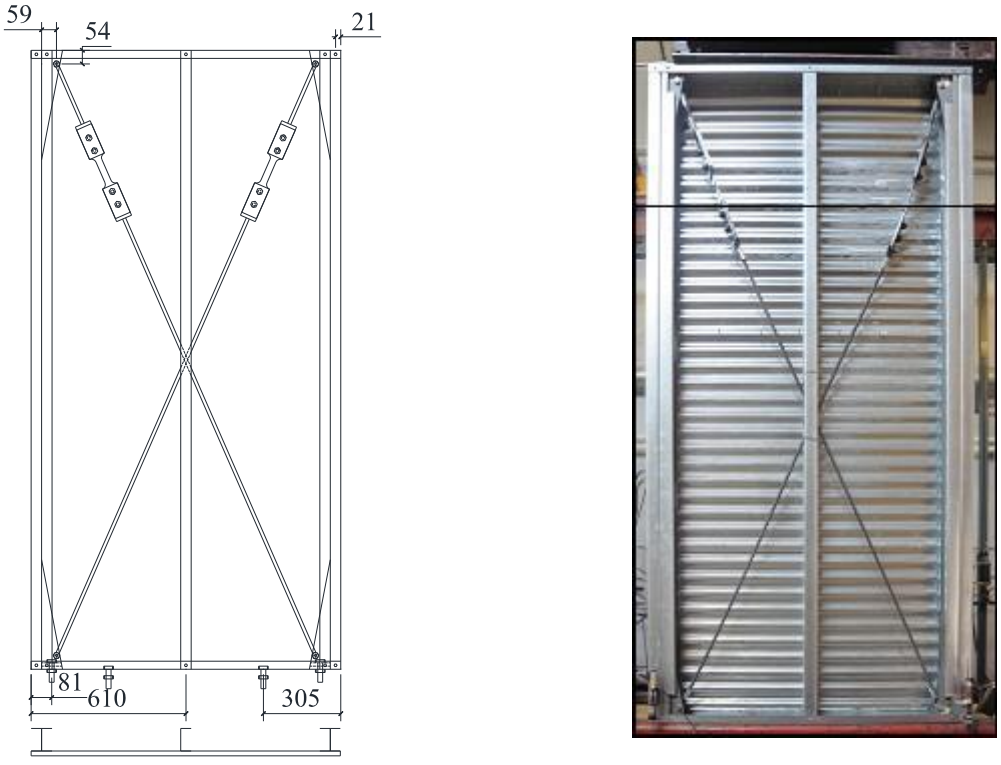

Figure 8: Layout of the shear walls structure (a) The back-view of CFS shear wall using EDB (b) The photograph of CFS shear wall using EDB

All EDB used in this research had the same nominal thickness of dog bone shape steel plate: 3.57 mm (9/64 in.). Two threaded rods were used in brace. The total length of rods was 1962 mm (77-1/4 in.). Two Grainger 19L335 (Grainger, Champaign, Illinois) rod ends were used at each end

of the diagonal brace. Four Grainger 1JA22 (Grainger, Champaign, Illinois) coupling nuts were used to connect each part of brace together. The holder was assembled by two 9.525 mm (3/8 in.) thick hot-rolled steel plates with two bolt holes as shown in Fig. 9. Four 12.5 mm (1/2 in.) diameter ASTM 325 (ASTM 2015) bolts were used to connect the dog bone shape steel plate to the holder.

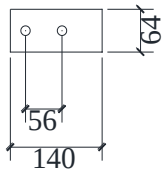

Figure 9: The dimension of holder plates

Coupon tests were conducted following the ASTM A370 (ASTM 2017) Standard test methods and definitions for mechanical testing of steel products to obtain the actual properties of the test materials. The coating on steel samples were removed with hydrochloric acid before testing. The coupon tests results are summarized in Table 2.

Table 2 Material properties

Component	Uncoated Thickness (mm)	Yield Stress F_y (MPa)	Tensile Strength F_u (MPa)	F_u/F_y	Elongation for 50.8 mm gauge length (%)
Stud	1.767	406.6	522.0	1.28	29.0
Track	1.772	380.5	530.7	1.39	54.5
Corrugated steel sheet	0.932	675.7	678.4	1.00	2.1
Dog bone shape steel plate	3.205	293.0	354.4	1.21	15.6

3. Test Result

3.1 Tested Shear Wall Properties

The performance parameters obtained from each wall specimen are provided in Tables 3 and 4. The results include the test peak load (P_{max}), lateral displacement at peak load (Δ_{max}), elastic load ($P_e = 0.4\ P_{max}$), ultimate load ($P_u = 0.8\ P_{max}$) and displacement (Δ_e, Δ_u) at 0.4 P_{max} (pre-peak) and 0.8 P_{max} (post-peak), initial stiffness, yield strength (P_y), lateral displacement at yield strength (Δ_y) (pre-peak), ductility factor, and dissipated energy. The ductility factor, P_y and Δ_y were calculated by using the equivalent energy elastic plastic model (EEEP) according to ASTM E2126 (ASTM 2012b) Standard Test Methods for Cyclic (Reversed) Load Test for Shear Resistance of Vertical Elements of the Lateral Force Resisting Systems for Buildings. The backbone curves in both the positive and negative displacement regions were first identified by plotting the locus of all the peak-force points at the first circle of the same amplitude cycles. Then the parameters were determined from the backbone curves. Dissipated energy was defined as the area of all hysteresis loops for cyclic tests. For monotonic test, the parameters were determined from the load-displacement curves. Dissipated energy was defined as the area under the P-Δ curves from the origin point to 0.8 P_{max} point.

Table 3 Monotonic test results for shear walls

Label	P_{max} (kN)	Δ_{max} (mm)	P_y (kN)	Δ_y (mm)	Δ_u (mm)	P_u (kN)	μ	K_e (kN/mm)	E (kJ)
SW4×8-MNB	60.99	74.96	54.69	42.51	75.14	48.79	1.767	1.286	2.949
SW4×8-M100	62.41	70.48	57.97	52.33	82.03	49.93	1.567	1.108	3.231
SW4×8-M075	64.50	103.7	58.72	52.83	119.40	51.60	2.260	1.111	5.461
SW4×8-M050	71.35	91.64	56.55	41.80	96.80	57.08	2.316	1.353	4.675

Table 4 Cyclic test results for shear walls

Label	P_{max} (kN)	Δ_{max} (mm)	P_y (kN)	Δ_y (mm)	Δ_u (mm)	P_u (kN)	μ	K_e (kN/mm)	E (kJ)
SW4×8-CNB	56.92	59.39	51.97	39.39	84.33	45.53	2.150	1.350	10.649
SW4×8-C000	68.93	75.73	60.98	46.95	88.85	54.96	1.982	1.348	10.800
SW4×8-C050	61.25	67.63	56.16	40.56	103.90	49.00	2.898	1.394	15.544
SW4×8-C075	62.25	63.66	57.02	43.33	99.51	49.80	2.319	1.328	11.926
SW4×8-C050H	68.05	79.02	60.43	46.50	117.03	54.44	2.517	1.300	12.246

3.2 Observed Shear Wall Behaviors

Behavior of shear walls without EBD: The shear wall specimens exhibited warping of the corrugated sheet in the initial stage of test loading. As the lateral displacement increased, the connection of the bottom sheathing failed as the warping of the corrugated sheet became more pronounced. The main failure modes were the buckling of the corrugated sheet, screw pulling over and pulling out from the sheathing at the boundary studs. It caused the shear strength dropped instantly. Test phenomenon of specimen SW4×8-M100 was similar to the wall without EDB. The reason for this is that sliding distance of EDB in specimen SW4×8-M100 was too long that the EBD did not bear loads during the test. Failure modes of these shear wall specimens are showed in Fig.10.

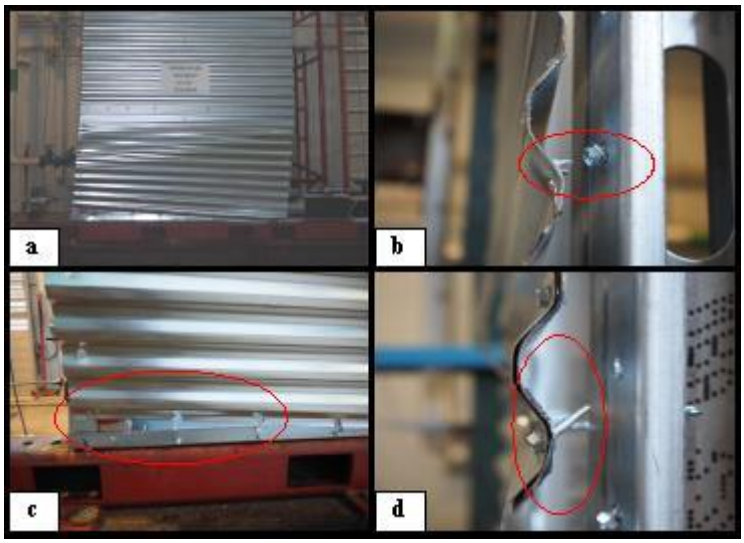

Figure 10: Failure modes of shear walls without EDB and SW4×8-M100 (a) sheet buckling (b) screw pulling over (c) screw hole tearing (d) screw pulling out

Behavior of shear walls with EBD: The failure modes were as same as the shear walls without EBD, including the buckling of corrugated steel sheathing and the failure of screw connection.

The dog bone shape steel plate deformed and yielded or broke in the last stage of testing due to large displacement amplitude. The EBD was able to provide supplemental shear strength after the failure of screw connections until the dog bone thin steel plate yielded. Therefore the shear walls could maintain a relatively high shear capacity after the peak load until the EBD failed. Failure modes of shear walls with EDB are showed in Fig. 11. Table 5 shows the failure modes of all specimens.

Figure 11 Failure modes of shear walls with EDB (a) sheet buckling (b) screw pulling over (c) screw pulling out (d) EDB yielding (e) EDB fracturing

Table 5 Summary of failure modes of specimens

Test Label	Failure modes			
	Sheet buckling	Screw pulling over	Screw pulling out	EDB failure
SW4×8-MNB	√	√	√	-
SW4×8-M100[a]	√	√	√	none
SW4×8-M075	√	√	√	yielding
SW4×8-M050	√	√	√	yielding
SW4×8-CNB	√	√	√	-
SW4×8-C000	√	√	√	yielding
SW4×8-C050	√	√	√	yielding
SW4×8-C050H	√	√	√	fracture
SW4×8-C075	√	√	√	yielding

3.3 Discussion

Identical specimens were compared under monotonic and cyclic loadings. The load-displacement curves of both configuration under different loading methods are shown in Fig. 12. The failure modes and mechanism of the specimens in cyclic tests were similar to those in monotonic tests. Table 6 lists the shear strength of the shear wall under monotonic lateral loading compared with the average peak loads of the identical shear wall under cyclic loading, along with lateral displacement at peak load and ductility comparison. The average peak load of cyclic tests was 91.9% of the peak load of monotonic tests. This indicated the extent of the strength degradation in the cyclic loading protocol. The lateral displacement at peak load under cyclic loading was 71.4% of those under monotonic loading. The average ductility of cyclic tests has increased by

16.4% compared with those under monotonic loading. The loading method has more impact on the deformation capacity of specimens than the other mechanical properties. The results indicated that the specimens under cyclic loading accumulated more damages than the shear walls under monotonic loading which could cause the peak of the curve occurred early. Therefore, the behavior of post-peak has been influenced by the loading methods. As shown in Fig.12(c), Tables 3 and 4, the performance of specimen of half cyclic test (UNT protocol) was similar to that under cyclic loading. For this reason, the half cyclic test can be used to investigate the post-peak hysteresis behavior, particularly in the long displacement range.

Table 6 Comparison between monotonic test and cyclic test results

Label	P_{max} (kN)		P_{max2}/P_{max1}	Δ_{max} (mm)		$\Delta_{max2}/\Delta_{max1}$	μ		μ_2/μ_1
	Monotonic P_{max1}	Cyclic P_{max2}		Monotonic Δ_{max1}	Cyclic Δ_{max2}		Monotonic μ_1	Cyclic μ_2	
NB	60.99	56.92	0.933	74.96	59.39	0.792	1.77	2.15	1.215
075	64.50	62.25	0.965	103.70	63.66	0.613	2.26	2.32	1.027
050	71.35	61.25	0.858	91.64	67.63	0.738	2.32	2.90	1.250
Average value			0.919			0.714			1.164

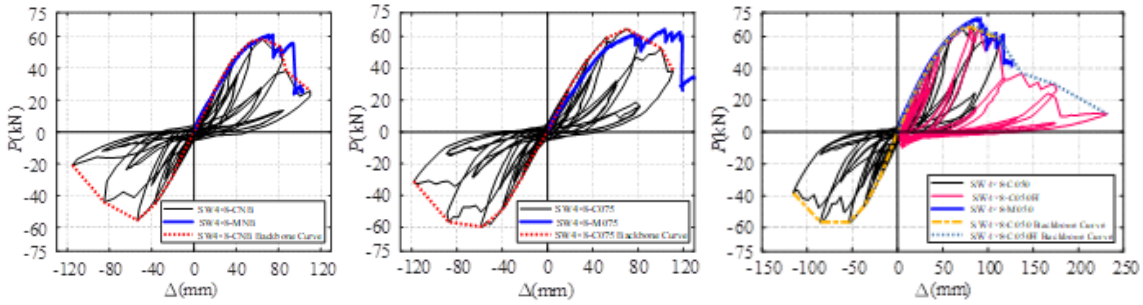

(a) (b) (c)

Figure 12 Comparison of monotonic loading and cyclic loading (a) Specimens without EDB (b) Specimens with EDB (sliding distance: 19.05 mm) (c) Specimens with EDB (sliding distance: 12.70 mm)

The impact of different sliding distance of EDB was of great interest in this research. A comparison analysis was made between specimens under cyclic tests with different sliding distance of EDB in the peak load, the ductility, the energy dissipation, and the equivalent ultimate drift. Based on the test result of specimen SW4×8-CNB, the seismic performance parameters of other specimens were normalized. Table 7 and Fig. 13 shows that the normalization result of peak load, ductility, energy dissipation and ultimate displacement. The scaling factor in Fig. 13 is the ratio of specific wall to SW4×8-CNB for those parameters investigated.

Table 7 The normalization results of seismic performance of specimens

Parameter \ Label	CNB	CNB/CNB	C000	C000/CNB	C050	C050/CNB	C075	C075/CNB
P_{max}(kN)	56.92	1.00	68.93	1.211	61.25	1.076	62.25	1.094
Δ_u(mm)	84.33	1.00	88.85	1.054	103.90	1.232	99.51	1.180
μ	2.150	1.00	1.982	0.922	2.898	1.348	2.319	1.078
E(kJ)	10.649	1.00	10.800	1.014	15.544	1.460	11.926	1.120

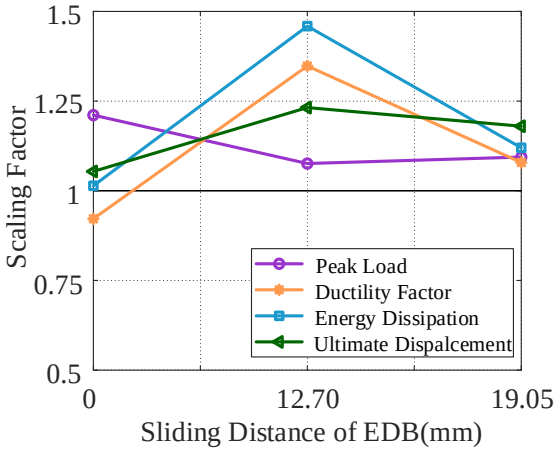

Figure 13: Effect of different sliding distance of EDB on seismic performance of specimens

The EDB was designed to improve the ultimate deformation capacity and ductility of CFS shear walls with corrugated steel sheathing. The results indicated that the sliding distance of EDB had a significant impact on the ultimate deformation capacity of specimens. As shown in Fig. 13, the ductility of SW4×8-C050 and SW4×8-C075 had increased noticeably by 34.8% and 7.9% respectively than standard specimen (SW4×8-CNB) because the EDB was engaged in the load bearing with the failure of the sheathing at approximately the same time. The EDB could effectively delay the instant dropping of load of the shear wall until the failure of the EDB. However, the ductility of SW4×8-C000 had decreased to 92.2% of the standard specimen. This is because the EDB engaged in the load bearing as soon as the loading started (zero sliding distance) and yielded before the peak load. The EDB could not provide additional stiffness and strength in the post-peak stage. The shear resistance capacity dropped instantly after peak. According to the definition of ductility coefficient, the ductility of the specimen (SW4×8-C000) is lower than that of the standard specimen (SW4×8-CNB).

The energy dissipation capacity of specimens under cyclic loading is also an important parameter for evaluating the seismic performance of CFS shear walls. Dissipated energy was defined as the area of all hysteresis loops for cyclic tests. Fig. 13 shows the impact of different sliding distance of brace to energy dissipation of specimens. Compared with the standard specimen, the energy dissipation value of SW4×8-C050 had increased by 45.9%. Compared with other specimens which have the different sliding distance of EDB, the energy dissipation of SW4×8-C050 was 43.9% higher than SW4×8-C000 and 30.3% higher than SW4×8-C075. The reason for this is that EDB in SW4×8-C050 started to take part in load bearing as the shear wall approaching the peak load. Instead of instant failure, the shear wall and EDB worked together which led to a postponed peak load and an increase in ultimate deformation. The energy dissipation capacity was consequently enhanced. While due to the increased sliding distance, EDB in SW4×8-C075 took effect after the wall reached its peak point. The peak load and the corresponding displacement therefore did not change much. However, the EDB did delay the instant drop in shear strength by providing additional stiffness and strength in the post-peak stage. The energy dissipation capacity was thus enhanced, but not as much as SW4×8-C050. All of the three walls experienced warping in the corrugated sheets and SW4×8-C050 showed more significant deformation in the sheathing.

Fig. 13 also shows the ultimate displacement of specimens. The ultimate displacement of specimens had increased, especially specimen SW4×8-C050. The ultimate displacement of SW4×8-C050 was approximately 1.23 times of the specimen without EDB. The increment of other configuration walls was lower than 20%.

As shown in Fig. 13, the peak load of SW4×8-C000, SW4×8-C050 and SW4×8-C075 had increased by 21.1%, 13.1%, and 11.2% respectively. Therefore, the peak load of all of the specimens has been improved to a certain extent. However, it is recommended that the contribution of EDB to the strength of shear walls shall not be taken into account in design, instead it could be considered as a safety reserve of the lateral strength. In order to evaluate the ultimate deformation capacity of each specimen at the same load level, a new parameter of equivalent ultimate drift (γ_{uE}) was proposed in this research. The parameter is defined as the corresponding drift on load-drift curve at 45.53 kN, which is the ultimate load of the specimen SW4×8-CNB. Fig. 14 shows the comparison of equivalent ultimate drift of different configuration shear walls. Compared with the standard specimen, the equivalent ultimate drift of SW4×8-C075 and SW4×8-C050 increased by 24.2% and 47.7%, respectively. The backbone curve of SW4×8-C050 was replaced by SW4×8-C050H because SW4×8-C050 did not have the ultimate displacement point due to the limit of the displacement range of the actuator.

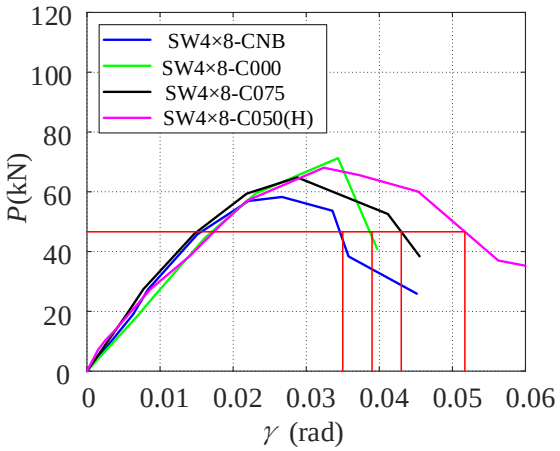

Figure 14: Equivalent ultimate drift of specimens

The analysis results indicate that the sliding distance of EDB is of great importance and EDB with optimized sliding distance can greatly improve the seismic performance of the CFS shear wall with corrugated steel sheathing. The ductility, ultimate deformation capacity and energy dissipation of CFS shear wall with appropriate EDB can be improved without the reduction in strength, initial stiffness, fire rating, and other non-structural properties. The CFS shear wall with EDB with optimized parameters can be a high-strength high-ductility lateral system for mid-rise CFS framed buildings in seismic zones.

4. Conclusions

In this paper, a special energy dissipative brace (EDB) is proposed to improve the ductility of corrugated shear walls without changing the initial stiffness and peak load of the wall. To investigate the effect of EDB on the seismic performance of corrugated shear walls, a series of

full-scale shear wall tests were conducted in this project. It was found that the working mechanism of EDB relied on the sliding distance in the dog bone shape thin plate. The EDB with optimal sliding distance could significantly enhance the performance of the post-peak stage of shear walls. The ductility and energy dissipation of the tested shear walls were effectively improved, and their stiffness degradation after peak load was retarded. The proposed EDB could be a viable solution for the application of cold-formed steel shear walls with corrugated steel sheathing in high seismic risk zones.

5. References

ASTM A370 (2017). "Standard test methods and definitions for mechanical testing of steel products", *American Society for Testing and Materials*, West Conshohocken, PA.

ASTM E2126 (2012). "Standard test methods for cyclic (reversed) load test for shear resistance of vertical elements of the lateral force resisting systems for buildings", *American Society for Testing and Materials*, West Conshohocken, PA.

ASTM E564 (2012). "Standard Practice for Static Load Test for Shear Resistance of Framed Walls for Buildings", *American Society for Testing and Materials*, West Conshohocken, PA.

ASTM E3125/F3125M-15a (2015). "Standard specification for high strength structural bolts, steel and alloy steel, heat treated, 120 ksi (830 MPa) and 150 ksi(1040 MPa) minimum tensile strength, inch and metric dimensions", *American Society for Testing and Materials*, West Conshohocken, PA.

Franklin, N., E. Heffernan, and T. McCarthy. (2020). "The case for cold-formed steel construction for the mid-rise residential sector in Australia: A survey of international CFS professionals." *ACMSM25*. Springer, Singapore, 841-851.

Fülöp, L.A., and Dubina, B. (2004). "Performance of wall-stud cold-formed shear panels under monotonic and cyclic loading Part I: Experimental research", *Thin-Walled Structures*, Elsevier, 42(2), 321-338.

Liu, P., Peterman, K. D., and Schafer, B. W. (2014). "Impact of construction details on OSB-sheathed cold-formed steel framed shear walls". *Journal of Constructional Steel Research*, Elsevier, 101, 114-123.

Shamim, I., Morello, D., and Rogers, C. (2010). "Dynamic testing and analyses of wood sheathed/CFS framed shear walls". *Proceedings of the 9th U.S. National and 10th Canadian Conference on Earthquake Engineering*, Toronto, Canada.

Serrette, R., and Ogunfunmi, K. (1996). "Shear resistance of gypsum-sheathed light-gauge steel stud walls." *Journal of Structural Engineering*, ASCE, 122(4), 383-389.

Serrette, R. L., Encalada, J., Juadines, M., and Nguyen, H. (1997). "Static racking behavior of plywood, OSB, gypsum, and fiberbond walls with metal framing." *Journal of Structural Engineering*, ASCE, 123(8), 1079-1086.

Serrette, R. L., Nguyen, H., and Hall, G. (1996). "Shear wall values for light weight steel framing." *Rep. No. LGSRG-3-96*, Santa Clara Univ., Santa Clara, CA.

Serrette, R.L. (1997). "Additional Shear Wall Values for Light Weight Steel Framing." *Report No. LGSRG-1-97*, Santa Clara University. Santa Clara, CA.

Serrette, R.L. (2002). "Performance of cold-formed steel-framed shear walls: Alternative configurations." *Final Rep.: LGSRG-06-02*, Santa Clara Univ., Santa Clara, CA.

Stojadinovic and Tipping (2007). "Structural testing of corrugated sheet steel shear walls." *Report submitted to Charles Pankow Foundation*, Ontario, CA.

Selvaraj, S., and Madhavan, M. (2018). "Studies on cold-formed steel stud panels with gypsum sheathing subjected to out-of-plane bending." *Journal of Structural Engineering*, ASCE, 144(9), 04018136.

Selvaraj, S., and Madhavan, M. (2019). "Bracing effect of sheathing in point-symmetric cold-formed steel flexural members." *Journal of Constructional Steel Research*, Elsevier, 157, 450-462.

Selvaraj, S., and Madhavan, M. (2019). "Investigation on sheathing effect and failure modes of gypsum sheathed cold-formed steel wall panels subjected to bending." *Structures*, Elsevier, 17, 87-101.

Selvaraj, S., and Madhavan, M. (2019). "Sheathing bracing requirements for cold-formed steel wall panels: experimental investigation." *Structures*, Elsevier,19, 258-276.

Selvaraj, S., and Madhavan, M. (2020). "Structural behavior and design of plywood sheathed cold-formed steel wall systems subjected to out of plane loading." *Journal of Constructional Steel Research*, Elsevier, 19, 105888.

Vieira Jr, L. C. M., and Schafer, B. W. (2013). "Behavior and design of sheathed cold-formed steel stud walls under compression." *Journal of Structural Engineering*, ASCE, 139(5), 772-786.

Yu, C. (2010). “Shear resistance of cold-formed steel framed shear walls with 0.686-mm, 0.762-mm, and 0.838-mm steel sheet sheathing.” *Engineering Structures*, Elsevier, 32, 1522-1529.

Yu, C., and Yu, G. (2016). “Experimental investigation of cold-formed steel framed shear wall using corrugated steel sheathing with circular holes.” *Journal of Structural Engineering*, ASCE, 10.1061/(ASCE)ST.1943-541X.0001609, 04016126.

Yu, C., Zhang, W., Yu, G., and Wang J. (2018). “Cold-formed steel framed shear wall using corrugated steel sheathing with slits.” *Journal of Structural Engineering*, ASCE, 144 (8): 04018111. https://doi.org/10.1061/(ASCE)ST.1943-541X .0002097.

Yu, G. (2013). “Cold-formed steel framed shear wall sheathed with corrugated steel sheet.” M.S. thesis, University of North Texas, Denton, TX.

Ye, J., Wang, X., and Zhao, M. (2016). “Experimental study on shear behavior of screw connections in CFS sheathing.” *Journal of constructional steel research*, Elsevier, 121, 1-12.

Zhang, W., Mahdavian, M., and Yu, C. (2018) “Different slit configuration in corrugated sheathing of cold-formed steel shear wall.” *Journal of Constructional Steel Research*, Elsevier,150, 430-441.